Chimney Formation in Solidifying Ga-25wt pct In Alloys Under the Influence of Thermosolutal Melt Convection

NATALIA SHEVCHENKO, STEPHAN BODEN, GUNTER GERBETH, and SVEN ECKERT

The directional solidification of Ga-25wt pct In alloys within a Hele-Shaw cell under the influence of thermosolutal convection was observed by means of X-ray radioscopy. The unstable density stratification at the solidification front causes the formation of rising plumes containing solute-rich liquids. The development of the chimneys and the probability of their surviving depend sensitively on the spatial and temporal properties of the flow field. Variations of the vertical temperature gradient along the solidification cell lead to the observation of different mechanisms for chimney formation. Perturbations of the dendritic structure are the origin of development of segregation freckles in case of low temperature gradients. The long-term stabilities of these segregation channels are strongly influenced by the transient nature of the melt convection. The situation at higher temperature gradients is characterized by two dominating convection rolls in the liquid phase which are driven by a lateral temperature gradient and the convex shape of the solidification front. The penetration of this flow pattern into the mushy zone results in continuous accumulation of solute in the central part of the mushy zone followed by a remelting of the solid fraction and the occurrence of a stable chimney.

DOI: 10.1007/s11661-013-1711-1

I. INTRODUCTION

SOLIDIFICATION processes are affected by natural convection as soon as instable density stratifications arise in the melt from local variations of the temperature and/or the concentration field. In particular, the rejection of solute at the solidification front which is lighter as the initial melt composition results in the formation of rising plumes in the liquid driven by the buoyancy force. Such convective plumes have been identified as the main reason for the development of solute-rich channels in solidifying metal alloys.[1–6] These channels may lead to freckle formation in fully solidified castings which is considered as a serious material defect deteriorating the mechanical properties of the final product.

Hellawell *et al.*[3] distinguished between two convective regimes. Immediately after the initiation of the solidification process, the so-called finger regime develops which consists of ascending, solute-rich fluid fingers with diameters comparable with the primary dendritic spacing. In the course of solidification when larger volumes of solute are rejected at the growth front, the fine-scale finger regime will be superseded by the occurrence of solute plumes showing lateral extensions up to a few interdendritic spacings. It is widely assumed that these large-scale plumes cause the channel segregation defects frequently observed in metal castings.

The fundamental description of the linear instability with respect to the melt convection in the situation of directional solidification was given by Worster.[7,8] He revealed the existence of two different modes of convective instability: a boundary layer mode, where the occurrence of convective cells is restricted to the liquid phase ahead of the solidification front, and a mushy-layer mode appearing at longer wave lengths, where the convection penetrates the entire mushy zone. The formation of the chimneys was attributed to the impact of the long-wavelength mushy-layer mode, which in turn will be triggered by a sufficiently strong convection in the liquid zone through the development of significant corrugations in the upper mushy layer. For reasons of continuity, rising plumes of solute-rich fluid in the liquid zone initiate an ascending flow also in the mushy layer beneath. Fluid in the lower mushy zone, which is enriched in the lighter solute, is mobilized and begins to rise into increasingly warmer zones, where it becomes undersaturated. Therefore, these interdendritic flows can dissolve the dendrites carving out chimneys into the porous dendritic network.

A strong coupling exists between melt flow and the solidification process. In the situation of an upward solidification, the pileup of the light solute component at the solid–liquid interface acts as the driving mechanism for the convection. In turn, the flowing melt redistributes the concentration field in the boundary layer and the mushy zone considerably. Besides the formation of segregation channels, such a modification causes dramatic changes in growth rate and direction of the dendrites, and influences the selection of the secondary dendrite branches.[9–11]

NATALIA SHEVCHENKO and STEPHAN BODEN, Research Fellows, GUNTER GERBETH, Institute Director, and SVEN ECKERT, Head of Magnetohydrodynamics Department, are with the Helmholtz-Zentrum Dresden-Rossendorf, Institute of Fluid Dynamics, P.O. Box 510119, 01314 Dresden, Germany. Contact e-mail: n.shevchenko@hzdr.de

Manuscript submitted November 16, 2012.
Article published online April 3, 2013

Many experimental investigations have been carried out using aqueous analogs as model liquids, which allow for a visual observation of convective flow pattern and chimney formation by diverse optical diagnostic techniques.[12–15] The dimensions of segregation channels occurring in such systems were shown to be comparable to those found by metallographic examinations in fully solidified metallic castings.[3] Although these similarities give point to extrapolate the findings from the transparent materials to metal alloys to a certain extent, corresponding measurements in real metallic materials are attractive as a further step toward full comparability. Real-time observations of solidification processes in opaque metal alloys can be realized by means of the X-ray radioscopic method. This technique enables real-time and in-situ observations of the solidification front with a spatial resolution of a few microns.[16–18] The dimension of the solute boundary layers ahead of the solidification front can also be derived from image processing.[11,19] Only a few studies have been done so far disclosing information with respect to the flow structure near the growth front. A real-time X-ray radioscopic density visualization system has been used by Koster *et al.*[20,21] to study natural convection in liquid gallium and gallium alloys. Based on local density differences arising from temperature gradients or gravitational stratification, this technique delivers qualitative pictures of the flow pattern. However, the spatial resolution achieved in these experiments was not sufficient to perceive details of the flow structure being in the order of the typical dendrite spacing. Boden *et al.*[11] employed the Optical Flow approach to acquire quantitative information about the liquid velocity field adjacent to the solidification front. For this purpose, they analyzed the displacement of the brightness patterns occurring between successive X-ray images.

The aim of the current study is to provide direct observations of the formation of segregation zones in opaque metallic alloys under the impact of thermosolutal convection. It is a continuation of a recent study by Shevchenko *et al.*[19,22] wherein first results concerning the development of chimneys in the mushy zone of a Ga-25wt pct In alloy were published.

II. EXPERIMENTAL METHOD

A. *Set-up of the Solidification Experiment and X-ray Technique*

The experimental setup is schematically depicted in Figure 1. The solidification experiments were carried out using a Ga-25wt pct In alloy [T_{Liquidus} = 298 K (25 °C), T_{Solidus} = 288.3 K (15.3 °C)] prepared from 99.99 pct Ga and 99.99 pct In. The alloy was contained in a capillary slit container made from quartz glass (see Figure 1(b)). Two glass plates (25 mm × 35 mm, thickness 2 mm) are aligned parallel with a gap of 150 μm. This Hele-Shaw cell is equipped with two pouring nozzles where the liquid alloy is filled into the cell by generating a suction pressure. This procedure avoids the occurrence of gas bubbles in the thin metallic film.

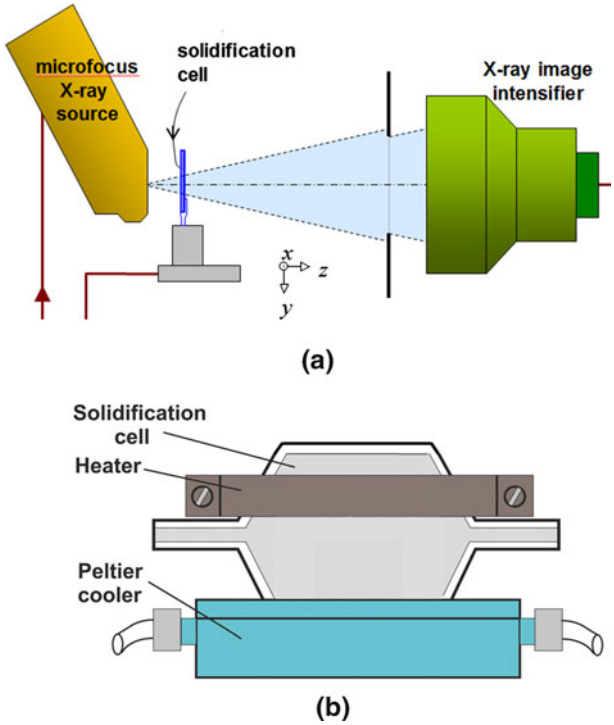

Fig. 1—Schematic view of the experimental setup: (*a*) X-ray diagnostic system; (*b*) Hele-Shaw solidification cell equipped with electric heater and Peltier elements.

In our study, the growth conditions are organized to be similar to those of Sarazin and Hellawell[2] or Bergman *et al.*[5] where the positions of both the furnace and the crucible were chosen to be stationary and base chilled. We used an electric heater mounted on the upper part of the solidification cell to heat up the alloy. The cooler is made of a linear array of Peltier elements being attached to the bottom part of the cell. In the course of the solidification the temperature gradient across the cell and the cooling rate were controlled by a simultaneous regulation of both the electric heater and the Peltier cooler. In our experiments we adjusted the cooling rate, whereas the temperature gradient G and the mushy zone height do not remain constant during the process. Two miniature K-type thermocouples (∅ 0.1 mm) were contacted to the face of the cell for monitoring the temperature during the process. We are able to measure the complete temperature field in additional experiments by an infrared camera (Trotec IC 080 LV) equipped with a LCD monitor and an image sensor having a resolution of 384 × 288 pixel. The experiments in the current article were carried out at cooling rates of 0.01 K/s and heating powers ranging from 0 to 1.7 W. Series of experiments have been realized applying multiple cycles of solidification and remelting processes.

The solidification experiments were monitored by an X-ray radioscopic set-up delivering images with a spatial resolution of a few microns.[11] A microfocus X-ray tube equipped with a tungsten target (phoenix X-ray XS225D-OEM) has been utilized. The X-ray tube generates a horizontally aligned divergent beam which penetrates the measuring volume. After passing the solidification cell, the attenuated X-ray beam impinges

an X-ray image intensifier (Thales TH9438HX 9''), where the X-rays are converted into a two-dimensional (2D) visible light distribution which is recorded by a CCD camera (Kappa CF8/1 BV-3) with a scan rate of 50 half frames per second. The camera signal is digitalized by a computer based frame grabber card. Consecutively acquired image frames are directly transferred into the computer for data processing. Single frames were integrated to reduce the noise level of the particular images. In our experiments presented here, an integration time of ~1 second was found to be sufficient to insure an adequate temporal sampling rate while keeping the amount of stored data manageable. Before post processing, each image frame was corrected taking into account the camera's dark current signal. Parallel to the image acquisition the CCD camera also delivers a live frame providing an online control of the process. In the present experiments, an X-ray tube voltage of 63 kV was chosen. Tube power was restricted to 9.4 W to insure a high spatial resolution, which is ultimately limited by the extent of the focal spot size. These specific parameters lead to a spatial resolution of 10 μm which has been verified by an additional reference measurement (not shown here).

The container position with respect to the beam was adjusted by means of a computer-controlled three-axis translation stage. The size of the measuring volume and the magnification ratio can be controlled by a suitable choice of the distances between the X-ray tube, the glass container and the X-ray image intensifier. In our experiments, the maximum field of view was 22.5 mm by 30 mm allowing the observation of both the dendrite structure of the solidifying alloy as well as the flow pattern appearing on a macroscopic scale. The bottom of the cell where the nucleation takes place is covered by the Peltier cooler. Therefore, it cannot be examined in the current study. The growing dendrites reach the field of view at 5 mm above the bottom of the solidification cell.

The solidification experiment was carried out as follows. At first, the binary Ga-25wt pct In-based alloy was melted and heated up to 308 K (35 °C), *i.e.*, 10 K above the liquidus temperature. The melting process was controlled by real-time radioscopic observation to insure a completely melted and homogenously distributed material before starting the solidification experiment. A homogeneous melt is considered to be achieved, if any transient changes of local intensities in the live frame have completely disappeared. Then, a reference image is computed by averaging the frames captured during this quasi-steady state. Thereafter, the cooling of the melt and the image acquisition was initiated.

B. *Analysis of Concentration Distributions and Flow Fields*

The output of the X-ray radioscopy delivers a 2D projection of the local density in the slit container corresponding to the distribution of the relative brightness P in the acquired images, which allows for an assessment of the local constitution inside the liquid phase. The use of the relative brightness in form of the normalized difference between the intensity at a respective pixel location and initial intensity before initializing the solidification prevents artifacts arising from marginal insufficiencies of the experimental configuration such as slight ripples of the glass container and compensates local beam brightness and detector efficiency variations. Therefore, the initial melt composition C_0 obviously corresponds to a relative brightness of zero. The local indium concentration inside the liquid phase can be determined by interpolation using a fitted rational function.[11]

Our analysis of the flow field in the present article follows the Optical Flow approach proposed by Horn and Schunck.[23] The applied algorithm to determine the optical flow from the X-ray images delivers reliable information concerning the velocity field in regions where sufficiently large brightness gradients occurs.[11] The solidification process creates differences of the local composition within the melt leading to characteristic pattern of transmitted light intensity. The analysis of the flow field relies on the monitoring of the temporal variations of characteristic brightness patterns in the liquid phase. Some specific results concerning the flow structures in the melt recovered by the Optical Flow approach have been published elsewhere.[11] It is pertinent to note that the assessment of the fluid velocity in segregation channels or in zones with an almost homogeneous solute concentration appears as very difficult using the Optical Flow algorithm.

III. RESULTS

A. *Measurements of the Temperature Field*

Within the frame of the current study we have carried out more than 25 experimental runs with three different temperature gradients being a consequence of different heating powers applied. Main solidification parameters of the respective experiments are presented in Table I.

Exemplary temperature fields measured by means of the infrared camera at the surface of the cell are presented in Figure 2. The isotherms in the melt are not ideally flat and not aligned perpendicularly with respect to the applied vertical thermal gradient. An additional lateral temperature difference arises from the specific hexagonal geometry of the solidification cell. The conical shape of the side walls does not allow for a perfectly uniform cooling of the sample. The extent of this lateral gradient depends on several parameters such as the heating power of the electrical heater, the applied cooling power or the distance between the heater and cooler position which was fixed at a value of 10 mm for all experiments presented in the current article. The horizontal temperature gradient causes a convex shape of the solidification front analog to the isotherms. This situation is prone to drive a thermal convection showing a radial component of the melt flow along the solidification front.

Figure 3 shows the development of the temperature gradients during the solidification. A continuous increase can be observed with the lapse of time which corresponds

Table I. Number of Observed Chimneys and Solidification Parameters for Different Heating Regimes at a Chosen Cooling Rate of 0.01 K/s (G Temperature Gradient in the Liquid Above the Solidification Front; V Solidification Rate; $\Delta T_{lateral}$ lateral temperature gradient; Π permeability of the mushy zone; Ra_m mushy-zone Rayleigh number)

Heating Power (W)	0	0.4	1.7
Number of Experiments	5	10	10
Chimney Formation	0	4 of 10	10 of 10
G (K/mm)	0.3–0.7	0.7–1.0	1.5–2.0
$\Delta T_{lateral}$ (K/mm)	0.02–0.15	0.1–0.2	0.3–0.5
V (μm/s)	15–20	~8	~5
Π (10^{-10} m^2)	8–22	11–19	13–18
Ra_m	158	335	537

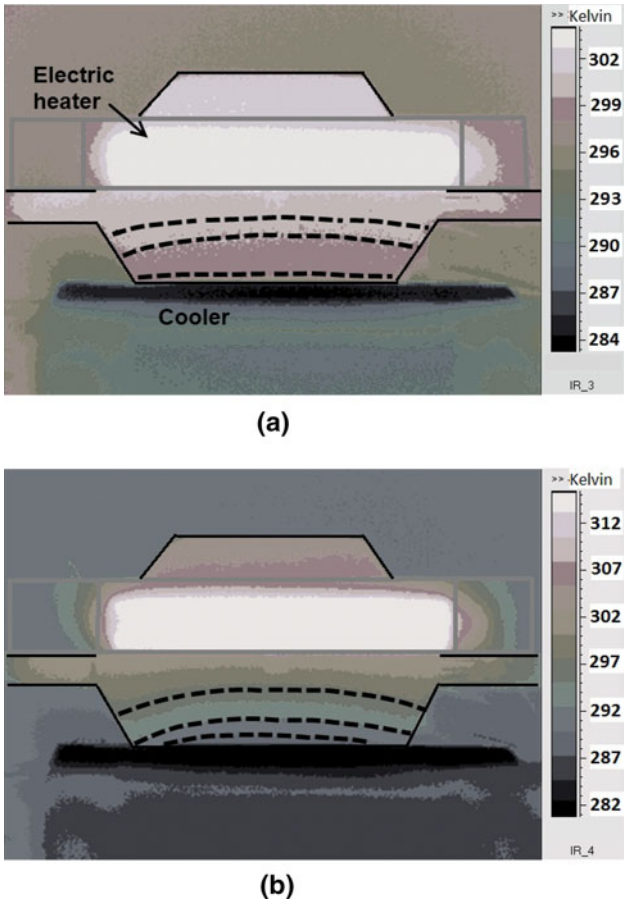

Fig. 2—Temperature distribution in a solidification cell obtained in experiments with different heating powers: (*a*) P_H = 0.4 W; (*b*) P_H = 1.7 W.[22]

to a reduction of the distance between the solid–liquid interface and the position of the electric heater. An enhancement of the heating power increases both the vertical and the lateral temperature gradient, too.

B. *Solidification at Low Temperature Gradients*

In a first step, we consider solidification experiments conducted without external heating (P_H = 0). This case

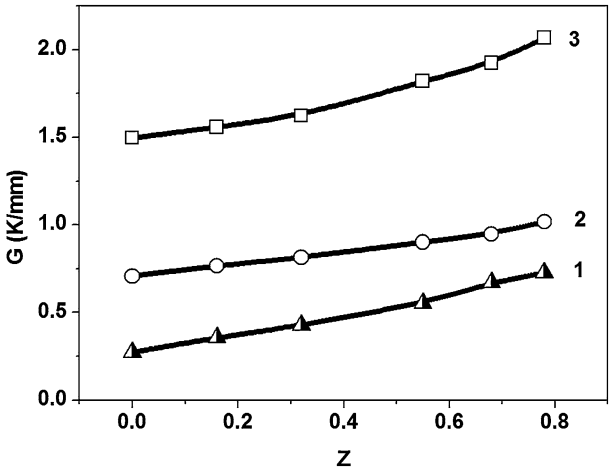

Fig. 3—Vertical temperature gradient *vs* position of solidification front at different heating powers: *1* P_H = 0; *2* P_H = 0.4 W; *3* P_H = 1.7 W.

is associated with low temperature gradients across the melt and a comparatively large undercooling region adjacent to the solidification front. Figure 4 displays a sequence of image frames recorded from the solidification process. The blue dendrites correspond to the primary Indium crystals (In-2wt pct Ga) which grow from the bottom of the cell. The solutal convection shows up in the form of rising Ga-rich plumes above the mushy zone. The velocity inside the ascending plumes was determined to be in the range of 50–130 μm/s. An erratic shape of the front is observed because of occurrence of the individual protruding dendrites. The microstructure appears to be fairly disordered across the image represented by the wide range of inclination angles of the dendrites with respect to the vertical line (5 deg–50 deg). The growth velocity of the dendrite tips reaches values of about 15–20 μm/s during the initial period of the solidification process.

Ga-rich plumes occur mainly right beside and above the protruding dendrites (see Figure 4(a)). The respective dendrites show an uneven growth of secondary arms. Their development is effectively suppressed in the area of a high solute concentration. Small equiaxed grains appear frequently in the undercooled liquid ahead of the dendritic front. Seemingly, several equiaxed grains nucleate near the rising plumes (see for instance the grains 1 and 2 in Figure 4(a)). However, our diagnostic system cannot detect tiny grains being smaller than 10 μm. Thus, it is possible that the nuclei originate in the mushy zone, where a partial solutal remelting may occur in the regions of solute pile-up. Secondary arms are detached from the primary trunks and transported by the ascending flow into the liquid region ahead of the mushy zone. Likely, the majority of these fragments will remelt completely within the Ga-enriched liquid of the rising plume. However, undercooled regions having a higher Indium concentration exist right beside the plumes. A rapid growth of equiaxed dendrites is observed if such tiny fragments leave the plume and reach these fluid regions. The developing crystals become heavier as the ambient melt and fall down until

their size reaches the gap of the solidification cell (see Figure 4(b)).

Figures 4(c) and (d) reveal the appearance of the first segregation zones inside the mushy layer. The formation of the segregation is triggered by the irregular growth of the dendritic network. Larger areas filled with Ga-rich interdendritic liquid can be observed between dendrites with divergent growth angles. Falling crystals affect the propagating solidification front. These equiaxed dendrites block open chimneys or growing dendrites (see for instance the grain 2 in Figure 4(d)). Moreover, the further growth of such crystals may provoke the formation of additional distinct plumes, which influences the local flows in the neighborhood. In a subsequent stage, the originally equiaxed grains are engulfed by the solidification front as it is shown on the right part of Figure 4(e) using the example of grain 2. The image in Figure 4(f) reveals the final irregular structure of the mushy zone without any preferential orientation of the dendrites with respect to the vertical thermal gradient. Many segregation freckles occur in the final state, their shape and distribution appears to be erratic. There is no open channel left in that experiment permeating throughout the entire mushy zone.

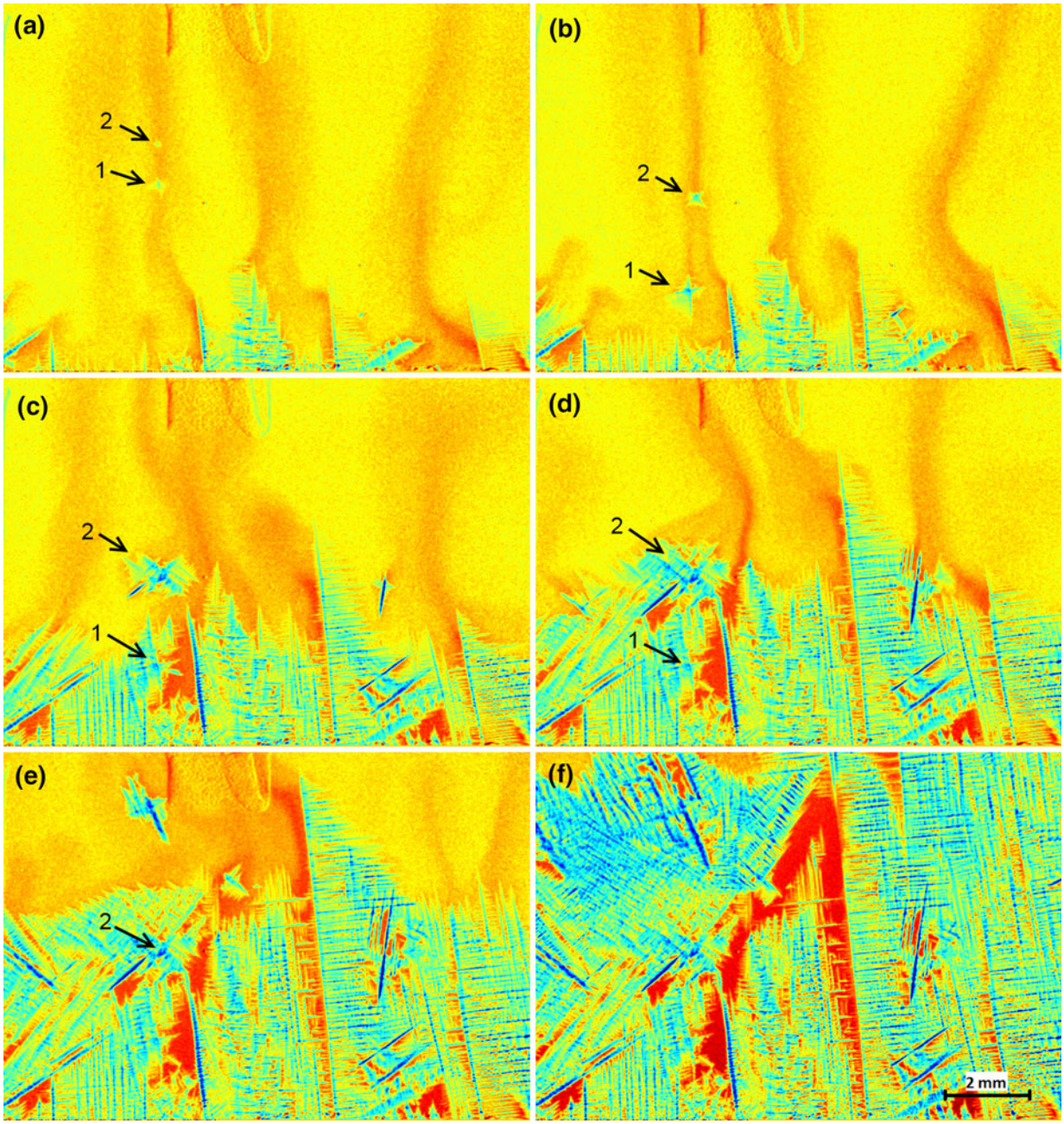

Fig. 4—Dendrite network and segregation freckle formation without additional heating ($P_H = 0$) at large undercooling region; series of selected images recorded at different time steps: (*a*) 115 s, (*b*) 135 s, (*c*) 200 s, (*d*) 260 s, (*e*) 360 s, (*f*) 750 s.

C. *Solidification at Medium Temperature Gradients*

Former investigations[22] have already revealed a distinct effect of the initial nucleation and the dendrite growth at the bottom of the solidification cell on the evolution of the vertical segregation channels. Here, we consider a typical scenario at a temperature gradient of 1 K/mm in Figure 5 containing a sequence of frames recorded from a solidification experiment at $P_H = 0.4$ W. The images document the propagation of a corrugated solidification front. Inclination angles of dendrites with respect to the vertical axis vary in the range between 5 deg and 25 deg. Figure 5(a) shows a few strong plumes within the field of view during the early stage of the experiment. During the process, a tendency can be noticed for approaching and merging of the plumes (see, for instance, the central part of the Figure 5(a)). A dominating plume might be further intensified by the attraction of smaller neighboring plumes. The positions of the plumes are associated with individual fast-growing dendrites behind which protrude from the growth front. The fast solidification at both sides of the plumes forms volcano-like structures (Figures 5(c) and (d)). Such volcanos characterized by an intensified solid growth around the mouth of an open segregation channel have been predicted by Felicelli *et al.*[6] by means of three-dimensional numerical calculations. This phenomenon indicates the existence of a vertical flow at the channel mouth initiated by the rising

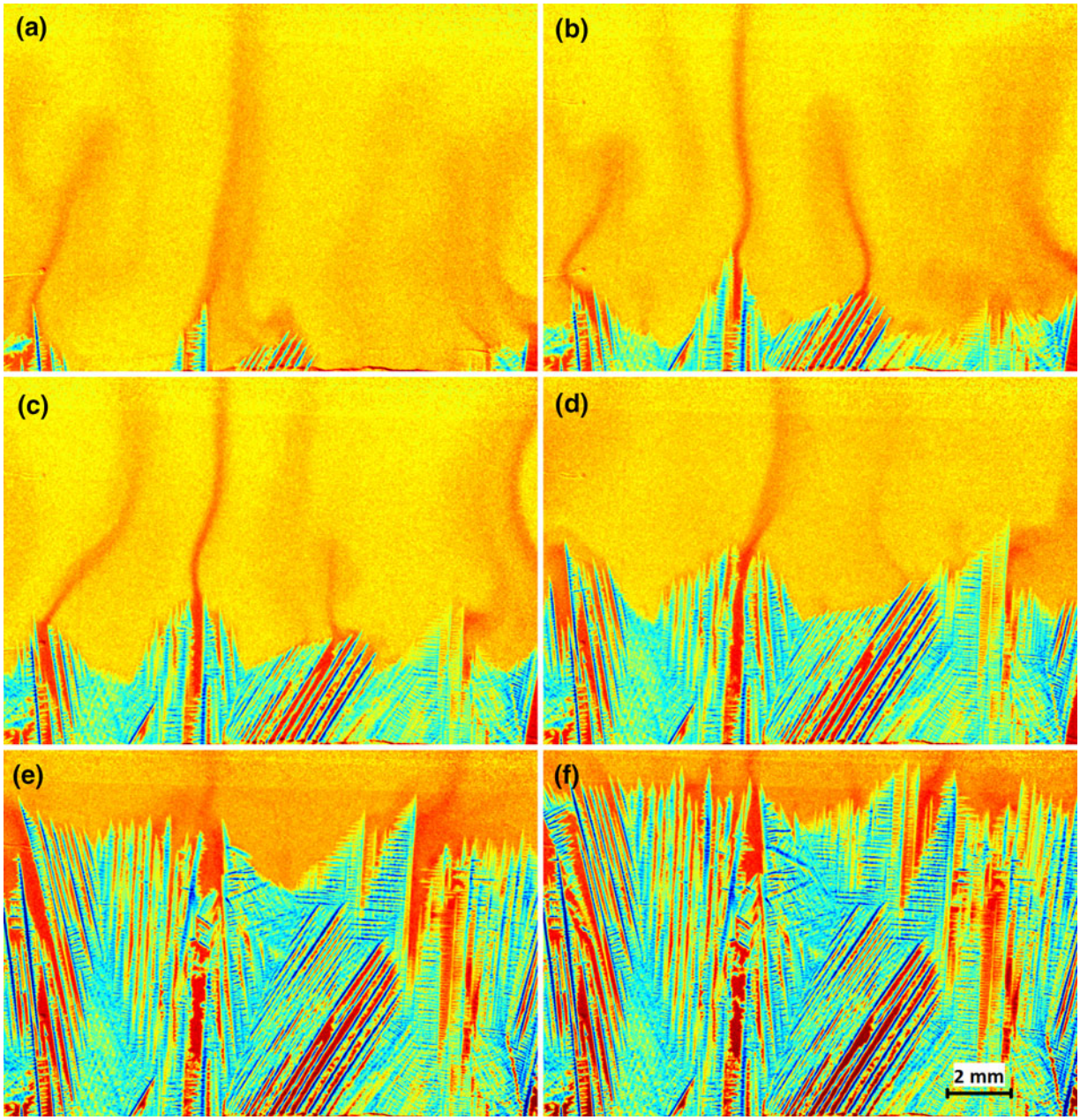

Fig. 5—Image sequence showing the dendrite growth and the formation of segregation freckles at medium heating power ($P_H = 0.4$ W); series of selected images recorded at different time steps: (*a*) 140 s, (*b*) 250 s, (*c*) 350 s, (*d*) 500 s, (*e*) 940 s, (*f*) 1200 s.

Ga-rich melt. Owing to the conservation of continuity, the plume generates an entrainment of fresh liquid from the side and below. The horizontal inflow brings more Indium toward the dendrites provoking the locally accelerated solidification.

The closer the dendrite axes are adjusted to the vertical line the higher the affinity was found to form open channels. As shown by Figure 5(d), the channel in the center becomes the dominating one, while the channel on the right-hand side is persistently blocked by overgrowing dendrite side arms. The stable segregation channel is associated with a strong plume at the chimney outlet. Solute-rich fluid rises through the channel and erodes surrounding dendrites. Sometimes, the remelting of the dendrites along the inner chimney walls cause the detachment of larger solid pieces from the dendritic network, which fall into the channel as it becomes apparent for the central channel in Figure 5(e). This blockage was not dissolved until the end of the experiment.

In summary, a temperature gradient up to 1 K/mm results in the formation of various segregation channels, but a sustainable development of stable chimneys was observed only in 4 of 10 experiments. Stable chimneys occur mainly at positions with initial growth defects or grain boundaries, however, not every initial segregation channel evolves into a stable chimney.

D. *Solidification at High Temperature Gradients*

Figure 6 shows a sequence of image frames recorded from the solidification process at a heating power of 1.7 W resulting in a higher temperature gradient up to 2 K/mm. This thermal condition restricts the undercooled region to a narrow zone adjacent to the solidification front. As a consequence, a rather smooth and even shape of the solidification front can be observed in Figure 6. Figures 6(a) through (c) shows a solidification cycle with almost no significant growth defect during a rather long initial period. Especially in the situation of the higher heating power regime we observe a converging flow ahead of the mushy zone from the cell edges to the center as shown in Figure 6(a) by black arrows. The continuous strengthening of the central plume causes a distinct solute accumulation in the mushy zone behind (Figure 6(d)). A remelting of dendrites happens Figure 6(e)) and the formation of a chimney can be detected (Figure 6(f)). This mechanism of chimney formation is different as compared to the case where the development of the segregation channel is linked with any initial growth defect as shown in the previous sections. These chimneys appear at a later stage of the solidification process and their extension is often restricted to the upper region of the mushy zone.

However, the other mechanism described in the previous section can also be found at high temperature gradients. A further example is displayed in Figure 7 containing a sequence of frames recorded at the same thermal boundary conditions as for the foregoing experiment. The origin of a segregation zone can be observed during the initial period of the solidification where a weak perturbation of the network can be detected (Figure 7(a)). Usually, such small channels show a rather volatile behavior, in particular they can migrate or disappear and re-emerge at another location.[19] Two parallel channels become visible on the right-hand side in Figure 7(b). The channel being located closer to the center is temporary blocked by the neighboring dendrites overgrowing the channel from the left-hand side. The strong solid growth is supported by the melt convection as mentioned above, whereas the dendrite side arms grow toward the flow coming from the right wall of the cell. At that time the right channel and the associated plume become rather strong. However, after about 1150 seconds fluctuations of the global melt flow occur which become apparent by a shift of the central plume toward the position of the blocked channel (Figure 7(c)). This change in the flow field results in a renewal of the chimney at the "old" location, the mouth becomes completely free by melting. Subsequently, a stable open channel is formed (Figure 7(d)).

In all solidification experiments performed under such conditions, at least one stable chimney can be detected. The analysis of our experiments revealed a remarkable tendency for a preferred chimney formation at the center as shown in the Figure 6. The occurrence of such central chimneys is promoted by the flow pattern ahead of the solidification front. The present examples clearly reveal that the development of the chimneys is strongly coupled with the advection of solute concentration by the melt flow. We can observe a converging flow ahead of the mushy zone leading to a concentration of the rising plumes in the central part of the solidification cell. The next paragraph will focus on the melt flow patterns ahead of the solidification front.

E. *Flow Patterns of Melt Convection Ahead of the Solidification Front*

A clear impact of the convection on the microstructure and the formation of chimneys becomes evident; however, the quantitative assessment of the melt convection impact is quite complex in detail.

Figure 8 shows two snapshots of the velocity field in the melt obtained by the Optical Flow approach for two applied temperature gradients. The image in Figure 8(a) displays the melt flow in the case of a temperature gradient of about 1 K/mm. This picture corresponds to the same time-step as shown in the Figure 5(b). Figure 8(a) reveals three fully developed plumes, which are related to individual fast-growing dendrites. The velocity inside the ascending plumes was determined to be in the range between 50 and 150 μm/s, whereas the magnitude of the flow velocity detected in the interdendritic region is considerably lower and reaches a maximum value of about 5–20 μm/s. The strong ascending flow requires a backfeed of fluid which generates an inward flow toward the center of the plume. Consequently, two vortices are formed on both sides of the plume. The strong flow component at the mouth of the open channel conveys In-rich liquid to the dendrite tips and enables an accelerated solid growth of the solid fraction there. The flow structure adjacent to the

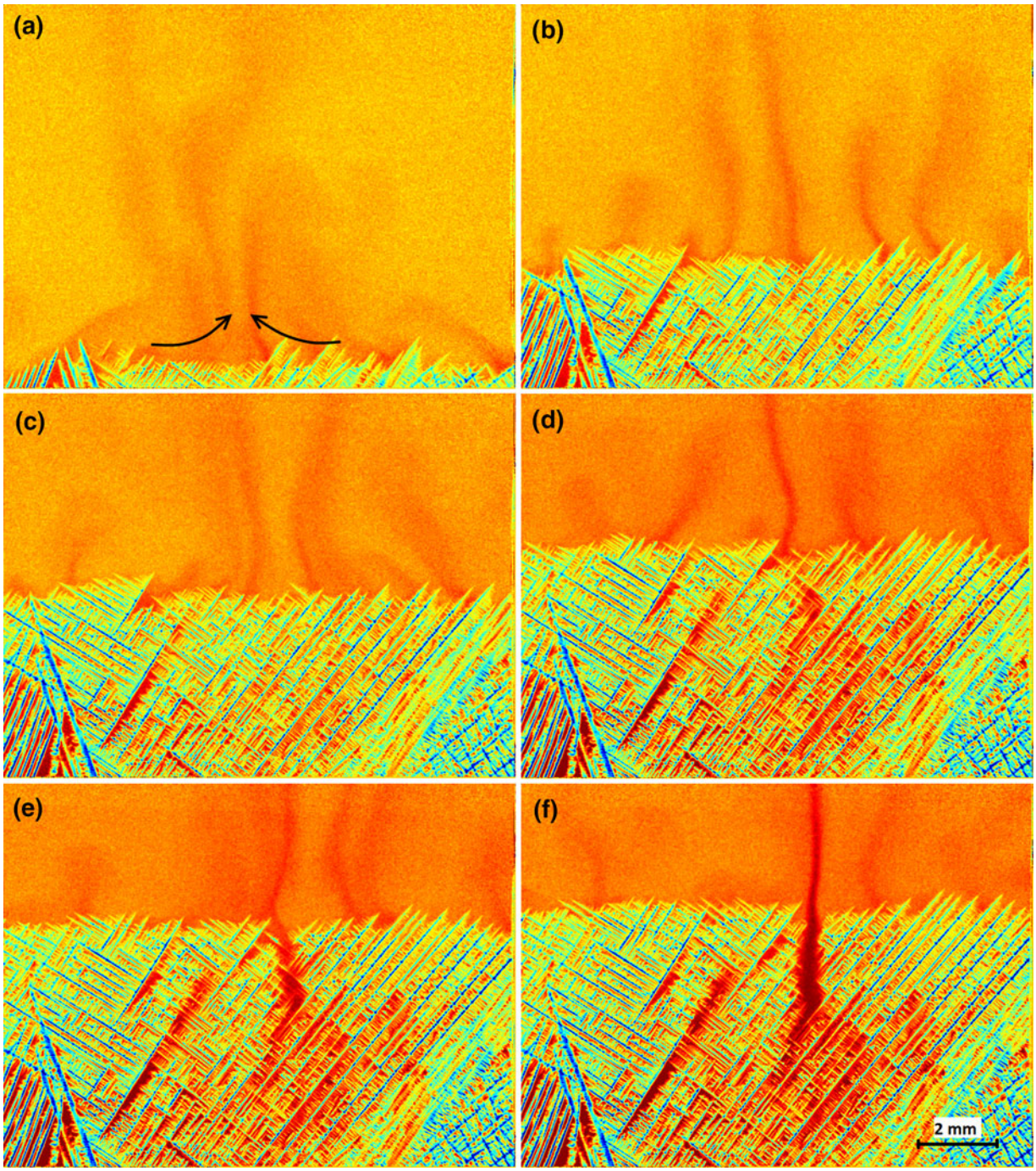

Fig. 6—Dendrite growth and chimney formation at higher heating power P_H = 1.7 W; snapshots recorded at different time steps: (*a*) 160 s, (*b*) 600 s, (*c*) 910 s, (*d*) 1260 s, (*e*) 1370 s, (*f*) 1500 s.

solidification front consists of vortex pairs to be grouped around the open channels.

In the case of higher heating power, we can identify a converging flow ahead of the mushy zone coming from the side walls and leading to a concentration of the rising plumes in the central part of the solidification cell. As shown in Figure 8(b), there occurs a global melt flow in the liquid zone consisting of two big convection rolls imposing a converging tangential flow along the solid–liquid interface. This double vortex flow spans over the entire cell volume. The velocities of the lateral flow close to the solidification front were determined to be in the range between 30 and 70 μm/s.

The Coanda effect describes the attraction of a fluid jet to a nearby surface.[24] This phenomenon results from the entrainment of ambient fluid around the jet and should also exist in case of two neighboring jets. The resulting lateral pressure causes a convergence of both jet positions. Such situations of approaching and merging of rising plumes can frequently be observed in

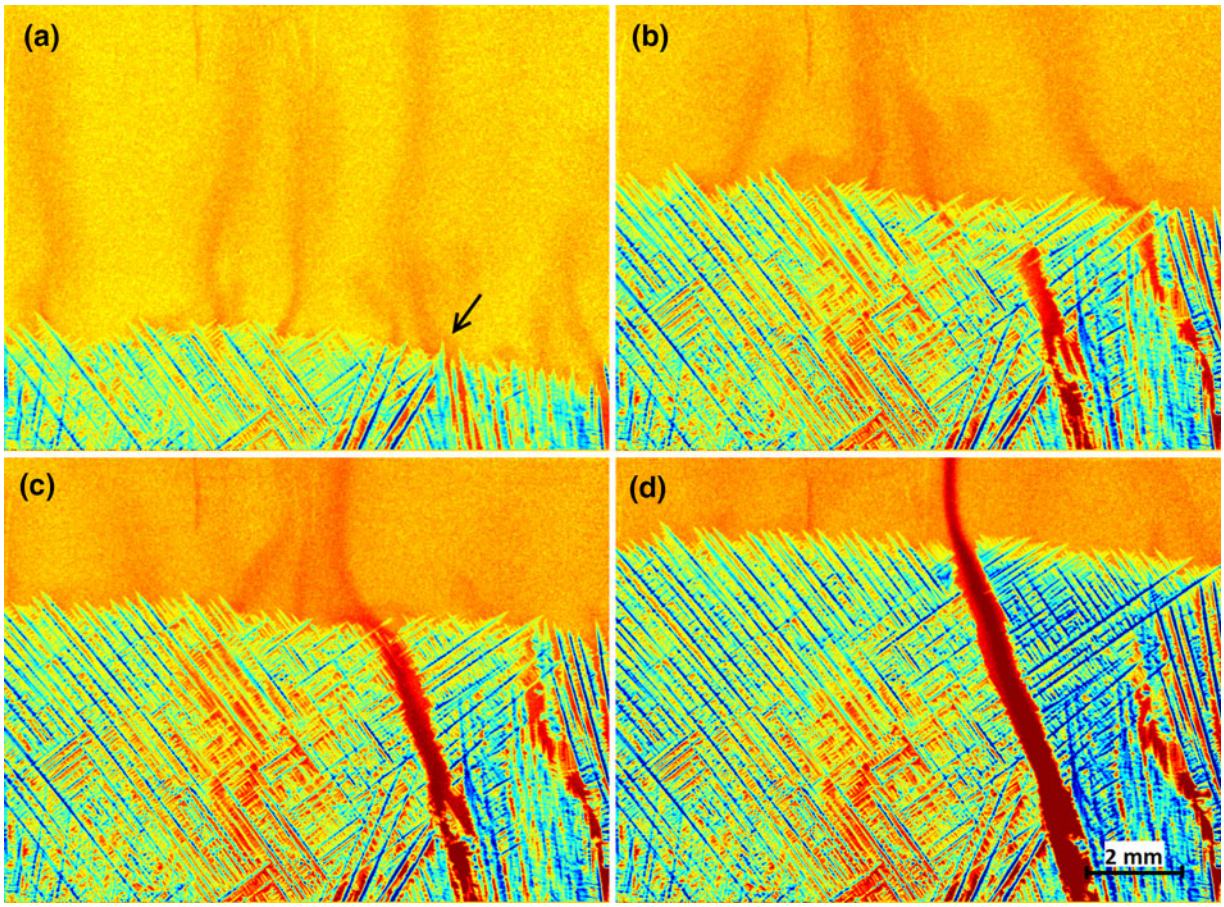

Fig. 7—Dendrite growth and chimney formation at small undercooling region at heater power $P = 1.7$ W; series of selected images recorded at different time steps: (*a*) 300 s, (*b*) 1000 s, (*c*) 1180 s, (*d*) 1600 s.

our experiments. Variations of the temperature gradient do not have an obvious influence on the number and the behavior of the plumes. The occurrence of the double-vortex convection in experiments at the high temperature gradient significantly conveys the plumes toward the central part of the solidification cell and promotes the establishment of a sustaining plume there.

Note that all experiments in the current study were performed in the range of a turbulent melt flow. Specific predictions concerning flow structure and the morphology of the solidified structure become difficult in case of transient or even turbulent convection. In general, the flow impact might be different for different regions of the mushy zone.

IV. DISCUSSION

Natural convection is driven by density differences in the fluid occurring because of gradients of the temperature or the concentration. The onset of convection in the liquid zone occurs when the non-dimensional Rayleigh number (Ra^{T}—thermal Ra number, Ra^{C}—solutal Ra number)

$$Ra^{T} = \frac{g\Delta\rho L^3}{\rho_0 \alpha \nu}; \quad Ra^{C} = \frac{g\Delta\rho L^3}{\rho_0 D_0 \nu} \qquad [1]$$

reaches a certain critical value (g and L stand for the gravity constant and the characteristic length scale, respectively, whereas ρ, α, D_0, and ν denote the density, thermal diffusivity, diffusion coefficient, and kinematic viscosity of the liquid, respectively). Moreover, the magnitude of the Ra number indicates whether the natural convection boundary layer is laminar or turbulent. Rough estimations for the considered alloy yield density differences of about 0.025 g/ cm^3 due to the global temperature drop in the cell and up to 0.3 g/cm^3 due to the concentration differences. Thus, the natural convection is mainly driven by the concentration gradients here. Under the experimental conditions considered in the current study the Ra^{C} number reaches a value in the order of 10^3 indicating a turbulent flow in the liquid bulk. The melt in the liquid zone is dominated by rising plumes of solute-rich melt. The formation of the plumes is in one way or the other influenced by the properties of the upper mushy zone, like the permeability, the spacing of the dendrites, and their growth angle with respect to the vertical axis. The continued existence of a plume needs a permanent entrainment of fluid from regions

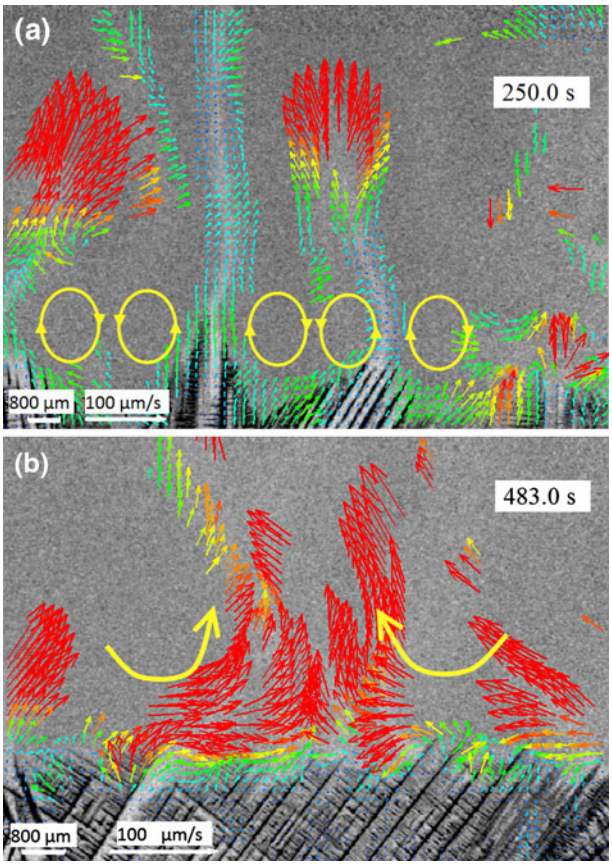

Fig. 8—Image frames showing the dendritic network and the related melt flow obtained by the optical flow approach at different heating powers: (*a*) 0.4 W; (*b*) 1.7 W.

around the plume. This creates a suction effect also in the mushy zone, which transports solute-rich interdendritic liquid toward the regions beneath the plume.

This interdendritic flow is considered to initiate the formation of freckle trails or chimneys. In order to find a critical threshold for the onset of chimney formation, the flow through the porous dendritic network should be taken into account by the modified so-called mushy-zone Rayleigh number Ra_m[7]

$$Ra_m = \frac{g\Delta\rho\Pi L}{\rho_0 \alpha \nu} = \frac{g\Delta\rho\Pi}{\rho_0 \nu V} \qquad [2]$$

Here, Π is the mean permeability of the mushy zone. There are several options to define the characteristic length scale L in Eq. [2]. Ramirez and Beckermann[25] evaluated various experimental data and concluded that good predictions of freckle formation can be obtained by using the ratio of the thermal diffusivity to the growth velocity as the length scale, *i.e.*, $L = \alpha/V$. This assumption was taken into account for writing the right hand side of Eq. [2]. Furthermore, the estimation of Ra_m needs an assessment of the permeability Π. Bergman *et al.*[5] suggested to set $\Pi = \delta^2$. The symbol δ denotes the interdendritic spacing which is understood as a mean fluid pathway between the dendrites through which the interdendritic liquid must flow.

We tried to determine a measure of Π by estimating the mean values of primary spacing λ_1 and solid fraction ε_S from our X-ray images. For calculating the mean permeability, we used the following equation proposed by Ramirez and Beckermann.[25]

$$\Pi = 0.074 \cdot \lambda_1^2 \cdot \left(\ln(\varepsilon_S) - 1.49 + 2 \cdot \varepsilon_S - 0.5 \cdot \varepsilon_S^2\right) \qquad [3]$$

For measuring ε_S, we followed an approach proposed by Delaleau *et al.*[26] who considered an idealized dendritic network composed of various cylinders. Each cylinder is considered to represent a respective primary or secondary arm. The length and the mean diameter of each arm were obtained by analyzing the microstructure from the radiograph. Furthermore, we assumed identical dimensions of the secondary arms growing parallel or perpendicular with respect to the X-ray beam at the same height of the primary trunk. Our analysis reveals large differences of the spacing between the dendrites (up to the factor of two) within one and the same sample. Therefore, the corresponding estimates for the mean solid fraction exhibit rather large local variations, which make a comparison between the experimental situations with different temperature gradients very difficult. Against this background, we decided to use a mean permeability of 15×10^{-10} m^2 for calculating Ra_m in all cases of heating powers applied here. Moreover, the evaluation of the radiographs is further complicated by the quality of the X-ray images which are affected by a limited resolution and an unsatisfying signal-to-noise ratio. Hence, we obtained mushy zone Rayleigh numbers of 158, 335, and 537 for the situations of low, medium, and high temperature gradients, respectively. The rising values of Ra_m with increasing temperature gradient are exclusively caused by the correspondingly decreasing growth rates of the dendrites.

The magnitude of the current study estimations for the mean permeability and the mushy zone Rayleigh number agrees well with the findings of Bergman *et al.*[5] for Pb-Sn alloys. In line with expectations, the tendency for forming chimneys strengthens with increasing Ra_m. However, in the cases studied here, the experimental observations point to the assumption that the mechanisms of chimney formation for the different thermal boundary conditions considered here differ from each other.

The solid structure within the mushy zone appears to be rather irregular in case of a low temperature gradient ($G < 0.7$ K/mm). Many perturbations of the dendritic network can be observed over the entire experiment, some of which show the potential to develop into temporary segregation zones showing a high amount of solute. The shape of these freckles is hardly predictable. The formation of chimneys seems possible only at locations beneath pronounced plumes. Such rising plumes are fed and kept alive by Ga-rich liquid from the mushy zone. In turn, the presence of the plumes prevents the ingress of In-rich fluid into the chimneys which would result in a rapid growth of the solid and a closing of the chimney. However, in the current study, the melt flow is turbulent, and strong fluctuations both of the growth process and the melt flow prevent the

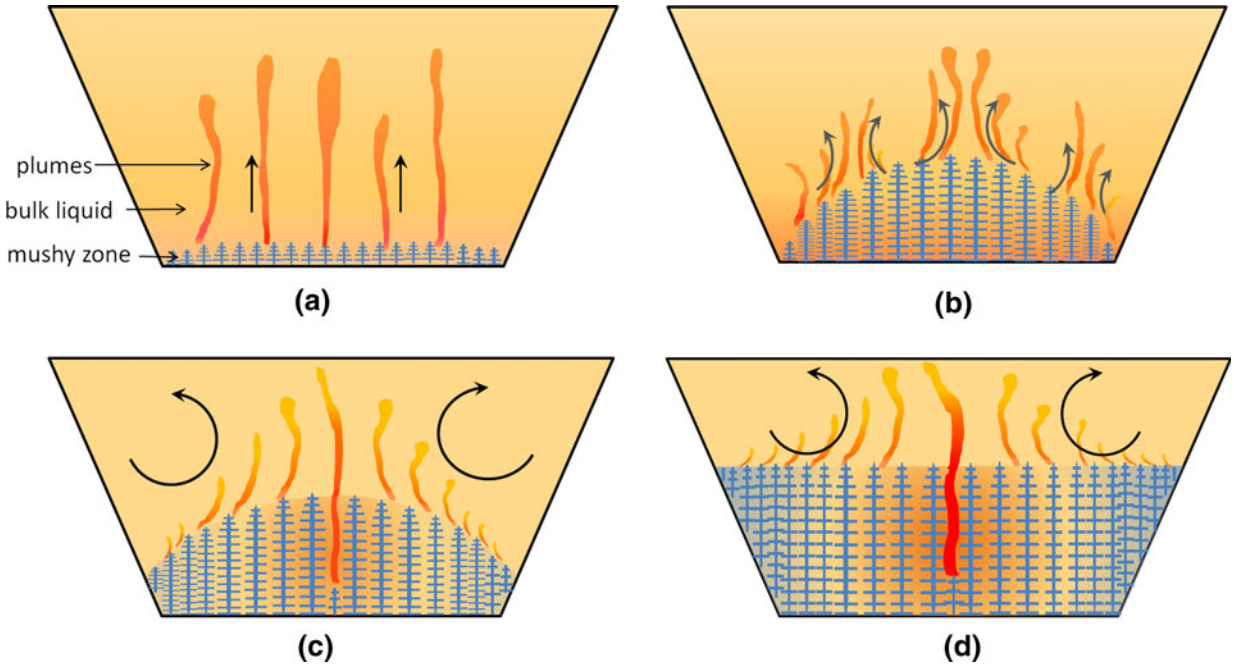

Fig. 9—Schematic illustration showing the mechanism of chimney formation.

manifestation of stable plumes and chimneys. Therefore, as shown in Figure 4, various freckles, but very seldom continuous chimneys, remain at the end of the experiment.

Continuous chimneys were obtained as a recurring phenomenon in the situation of high temperature gradients. The high temperature gradient provides a smooth shape of the solidification front. In the early stage of solidification, the solid fraction in the mushy zone grows rather regularly without any distinct perturbations. However, the special form of the solidification cell causes a lateral temperature gradient leading to a slightly convex shape of the dendritic front (see also Figure 2). According to Dantzig and Rappaz[27], we found for this configuration the initiation of an ascending flow of light solute-rich fluid along the solidification front from the side wall toward the center of the solidification cell. This flow structure becomes obvious by the lateral motion of the solutal plumes ahead of the mushy zone. Thus, the central plume becomes dominating and is further intensified by attracting and merging with neighboring plumes. The lateral inflow toward the center in the bottom part of the cell and the formation of a strong and stable rising jet ahead of the mushy zone drives a dominating double-vortex convection pattern inside the solidification cell which also has a deep impact on the dendritic network. This global double vortex flow penetrates the mushy zone and causes a solute enrichment in the central part of the solidification cell. The corresponding depression of the freezing point results in a dissolution of the dendritic structure by the inflowing liquid. At the same time the growth of the dendrites near the side walls of the solidification cell is promoted because solute-depleted melt reaches the dendrite tips there. This accelerated growth and the associated increase of the porosity of the mushy zone below the plume may further encourage the plume convection. This mechanism of chimney formations is schematically illustrated in Figure 9. As a result, a stable chimney appears in the central region of the solidification cell for all experiments conducted in the current study (see, *e.g.*, Figure 6(f)).

The experiments were carried out inside a thin Hele-Shaw cell, where the development of the melt flow is considerably restricted by the quasi-2D geometry of the configuration. The narrow gap of our solidification cell along the direction of the X-ray beam is further constricted by the growing dendrites. The permeability of the mushy zone is obviously lower as in a macroscopic three-dimensional experiment, which is why the melt flow experiences a higher flow resistance in the mushy zone. However, the analysis of our image sequences does show distinct transient changes of both the solute concentration in the intermediate space between the growing dendrites and the extent of the solid structures across the cell gap. This observation demonstrates that the flow paths in the interdendritic region are not completely obstructed. Melt flow also occurs in the intermediate area between the dendrites and the walls of the solidification cell. Therefore, the appearance of segregation channels is not absolutely suppressed, but, the chimney formation might be retarded by the almost 2D geometry as compared with the 3D case.

V. CONCLUSIONS

The current article presents an experimental study focusing on the initiation and development of segregation channels inside the mushy zone of a solidifying metal alloy under the influence of solutal melt

convection. A visualization of the solidification process and the main convection pattern in Ga-In alloys was obtained by means of the X-ray radioscopy as diagnostic tool. The visualization of the solidifying Ga-In alloys delivers simultaneous information of both the structure of the solid fraction in the mushy zone and the flow field especially in the vicinity of the solidification front. A sufficient understanding of the impact of melt convection on the formation of segregation channels in the solidified structure requires an authentic knowledge about the interaction between the dendritic growth and the solutal-driven flow. It becomes obvious from the experiments that crystallization of the dendrites and the melt convection are strongly coupled *via* the concentration field.

Main findings of the current study concerning the chimney formation can be summarized as follows:

1. Different scenarios have been observed concerning the formation of segregation channels in the mushy zone, which can be related to variations of the vertical temperature gradient along the solidification cell.
2. Variations of the temperature gradients applied over the solidification cell induce modifications of the melt flow pattern, which lead to different segregation structures.
3. Solidifications carried out at low temperature gradients revealed a considerable number of perturbations of the growing dendritic structure. Usually, such inhomogeneities are the starting point for developing segregation channels. The long-term stabilities of these segregation channels are strongly influenced by the transient nature of the melt convection.
4. The situation at higher temperature gradients is characterized by two dominating convection rolls in the liquid phase, which are driven by a lateral temperature gradient and the convex shape of the solidification front. The penetration of this flow pattern into the mushy zone results in a continuous accumulation of solute in the central part of the mushy zone followed by a remelting of the solid fraction and the occurrence of a sustaining chimney.

Future studies will focus on quantitative measurements of process parameters like the solid fraction, concentration field, and velocity structure. Such measurements require a better signal-to-noise ratio in the radiographs. Respective measures have already been initiated to achieve a corresponding improvement of the existing experimental equipment. Furthermore, systematic investigations are in progress wherein the influence of the lateral temperature gradient on the formation of segregation zones is considered in more detail.

ACKNOWLEDGMENTS

The current study was financially supported by the Deutsche Forschungsgemeinschaft (DFG) in the form of the Collaborative Research Centre SFB 609: ''Electromagnetic Flow Control in Metallurgy, Crystal Growth and Electrochemistry.''

REFERENCES

1. A.K. Sample and A. Hellawell: *Metall. Trans. A*, 1984, vol. 15A, pp. 2163–73.
2. J.R. Sarazin and A. Hellawell: *Metall. Trans. A*, 1988, vol. 19A, pp. 1861–71.
3. A. Hellawell, J.R. Sarazin, and R.S. Steube: *Phil. Trans: Phys. Sci. Eng*., 1993, vol. 345, pp. 507–44.
4. S.N. Tewari and R. Shah: *Metall. Mater. Trans. A*, 1996, vol. 27A, pp. 1353–62.
5. M.I. Bergman, D.R. Fearn, J. Bloxham, and M.C. Shannon: *Metall. Mater. Trans. A*, 1997, vol. 28A, pp. 859–66.
6. S.D. Felicelli, D.R. Poirier, and J.C. Heinrich: *Metall. Mater. Trans. B*, 1998, vol. 29B, pp. 847–55.
7. M.G. Worster: *J. Fluid Mech*., 1992, vol. 224, pp. 335–59.
8. M.G. Worster: *Ann. Rev. Fluid Mech*., 1997, vol. 29, pp. 91–122.
9. R. Trivedi, P. Mazumder, and S.N. Tewari: *Metall. Mater. Trans. A*, 2002, vol. 33A, pp. 3763–75.
10. J.E. Spinelli, D.M. Rosa, I.L. Ferreira, and A. Garcia: *Mater. Sci. Eng. A*, 2004, vol. 383, pp. 271–82.
11. S. Boden, B. Willers, S. Eckert, and G. Gerbeth: *Metall. Mater. Trans. A*, 2008, vol. 39A, pp. 613–23.
12. S.M. Copley, A.F. Giamei, S.M. Johnson, and M.F. Hornbecker: *Metall. Trans*., 1970, vol. 1, pp. 2193–2204.
13. B.T. Murray, A.A. Wheeler, and M.E. Glicksman: *J. Cryst. Growth*, 1995, vol. 154, pp. 386–400.
14. M. Zhang and T. Maxworthy: *J. Fluid Mech*., 2002, vol. 470, pp. 247–68.
15. S.H. Whiteoak, H.E. Huppert, and M.G. Worster: *J. Crystal Growth*, 2008, vol. 310, pp. 3545–51.
16. R.H. Mathiesen, L. Arnberg, F. Mo, T. Weitkamp, and A. Snigirev: *Phys. Rev. Lett*., 1999, vol. 83, pp. 5062–65.
17. R.H. Mathiesen and L. Arnberg: *Acta Mater*., 2005, vol. 53, pp. 947–56.
18. R.H. Mathiesen, L. Arnberg, K. Ramsoskar, T. Weitkamp, C. Rau, and A. Snigirev: *Metall. Mater. Trans. A*, 2002, vol. 33A, pp. 613–23.
19. N. Shevchenko, S. Boden, S. Eckert, and G. Gerbeth: *IOP Conf. Series: Mater. Sci. Eng*., 2011, vol. 27, p. 012085.
20. J.N. Koster, T. Seidel, and R. Derebail: *J. Fluid Mech*., 1997, vol. 343, pp. 29–41.
21. J.N. Koster, R. Derebail, and A. Grötzbach: *Appl. Phys. A*, 1997, vol. 64, pp. 45–54.
22. N. Shevchenko, S. Boden, S. Eckert, and G. Gerbeth: *IOP Conf. Series: Mater. Sci. Eng*., 2012, vol. 33, p. 012035.
23. B.K.P. Horn and B.G. Schunck: *Artif. Intell*., 1981, vol. 17, pp. 185–203.
24. D. J. Tritton: *Physical Fluid Dynamics*, Van Nostrand Reinhold, 1977 (reprinted 1980), Section 22.7, The Coanda Effect.
25. J.C. Ramirez and C. Beckermann: *Metall. Mater. Trans. A*, 2003, vol. 34A, pp. 1525–36.
26. P. Delaleau, C. Beckermann, R.H. Mathiesen, and L. Arnberg: *ISIJ Int*., 2010, vol. 50, pp. 1886–94.
27. J.A. Dantzig and M. Rappaz: *Solidification*, EPFL Press, Lausanne, 2009.